Tutors

Dr. Francesc Viñes Solana
Departament de Ciència de Materials i Química Física

Dr. Pablo Gamallo Belmonte
Departament de Ciència de Materials i Química Física

Grau de Química

Treball Final de Grau

Biogas upgrading by Grazynes
Enriquiment de biogàs mitjançant Grazins

Adrià Calzada Escrig

January 2021

Universitat de Barcelona

BKC Barcelona Knowledge Campus
Campus d'Excel·lència Internacional

Aquesta obra està subjecta a la llicència de:
Reconeixement–NoComercial-SenseObraDerivada

http://creativecommons.org/licenses/by-nc-nd/3.0/es/

La ciència es construeix amb dades, com una casa amb pedres. Però un conjunt de dades no és ciència, de la mateixa manera que un munt de pedres no és una casa.

Henri Poincaré

M'agradaria començar agraint a en Fransis i a en Pablo per la seva gran implicació i per haver-me ensenyat tant durant el procés de realització del treball. A tots els amics que m'han acompanyat durant aquests anys d'universitat i, sobretot, al meu pare, a la meva mare i a la meva germana, suport cabdal en tot el que faig.

REPORT

CONTENTS

1. SUMMARY

The present study focuses on the possible use of grazynes as membranes to separate biogas methane (CH_4) from carbon dioxide (CO_2), an impurity found when biogas is gained from the anaerobic digestion of organic matter. This is assessed by theoretical simulations using Density Functional Theory (*DFT*) in conjunction with the Perdew-Burke-Ernzerhof (*PBE*) exchange-correlation functional, and including a description of dispersive forces by means of Grimme D3 method (*PBE-D3*).

The analysis focused on the CO_2 and CH_4 diffusions through the pores of [1],[1]-, [2],[1]-, and [3],[1]-grazynes. To this end, adsorption energies for both molecules on two possible conformations were acquired as a matter of coverage and pore size, revealing that low-coverages are needed for a molecular diffusion, otherwise high-steric repulsions and diffusion energy barriers are found. As far as pore size is concerned, the larger the pore, the smaller the energy barriers. Aside, the interaction of the molecules with the grazynes is weak, mostly due to dispersive forces, which lower the adsorption energies and diffusion energy barriers. The study found that such grazynes are impermeable to both molecules, and only when achieving acetylenic defects on *c*(2×2) supercells, one could effectively expect a biogas upgrading.

There, the CO_2 molecule is found to trespass the membrane when overcoming energy barriers of *ca.* 0.5-0.6 eV when approaching with its molecular axis perpendicular to the grazyne pore. Diffusion is found to be impossible for other conformations, *e.g.* parallel CO_2, or any conformation of CH_4 molecule, revealing mechanisms of grazyne bulging out the impinging molecules, or, when forcing it, the observation of large deformations of the structure and/or the molecule. Thus, CO_2 could be 100% selectively separated when using defective [1],[1,2]{0,1}-, [2],[1,2]{0,1}-, and [3],[1,2]{0,1}-grazynes, enabling them to be used to get a purified methane stream in biogas upgrading.

Keywords: Grazynes, CO_2, CH_4, Biogas upgrading, Density functional theory, Adsorption energies, Diffusion energy barriers.

2. RESUM

El present estudi es centra en utilitzar grazins com a membranes per a separar el metà (CH_4) del biogàs del diòxid de carboni (CO_2), una impuresa que s'obté en la digestió anaeròbica de matèria orgànica. Això s'ha estudiat mitjançant càlculs teòrics de la teoria del funcional de la densitat, emprant el funcional de bescanvi i correlació de Perdew-Burke-Ernzerhof (*PBE*) incloent la descripció de les forces dispersives De feta per Grimme (*PBE-D3*).

El anàlisis es centra en les difusions de CO_2 i CH_4 a través de pors de grazins [1],[1]-, [2],[1]-, i [3],[1]-. Per a això s'han estimat les energies d'adsorció de totes dues molècules en dos possibles conformacions, en funció del recobriment i de la mesura de por, mostrant que hom requereix recobriments petits per tal d'evitar repulsions estèriques i tenir també barreres energètiques petites. En quant la mida de por, contra més gran és, mes baixa és la barrera. A part, la interacció de les molècules amb els grazins es feble, deguda principalment per forces dispersives, que fan baixar tant l'energia d'adsorció com les barreres energètiques. El estudi mostra que aquestes membranes son impermeables a totes dues molècules, a menys que es un faci servir cel·les *c*(2×2) amb defectes als contactes acetilènics, ja que aquests permetrien un enriquiment del biogàs.

En aquests materials s'ha trobat que la molècula de CO_2 pot traspassar la membrana, superant barreres energètiques de vora 0.5-0.6 eV quan la molècula de CO_2 s'apropa amb el seu eix perpendicular al grazí. Aquesta difusió s'ha trobat que es ben bé impossible per altres conformacions, com ara el CO_2 paral·lel, o qualsevol conformació del CH_4, mostrant en aquest casos mecanismes de deformació de la membrana per fer rebotar les molècules que hi arriben, o, quan es força, trobant grans deformacions del grazí o de les molècules. Així doncs, es pot separar el CO_2 del CH_4 amb una selectivitat del 100% quan es fan servir els grazins amb defecte [1],[1,2]{0,1}-, [2],[1,2]{0,1}- i [3],[1,2]{0,1}-, permetent el emprar-los com a membranes purificadores del metà en processos d'enriquiment de biogàs.

Paraules clau: Grazins, CO_2, CH_4, Enriquiment de biogàs, Teoria del funcional de la densitat, Energies d'adsorció, Barreres de difusió energètica.

3. INTRODUCTION

Pollution, global warming, industrial growth, and demographic rise are also pandemics that demand the constant search of renewable energies to mitigate their impacts. Thus, sustainable sources of energy are sought to avoid global warming and pollution, while being able to supply the energy to industry and to keep the standard of life of the growing population. One of these renewable sources with a promising future is biogas, a fuel derived from the anaerobic digestion of organic matter. Biogas is simply methane (CH_4), gained accompanied by some part of carbon dioxide (CO_2). Both molecules are indeed greenhouse gases, although to be more exact, there is 5% more CO_2 than CH_4 in the atmosphere, yet the later retains heat 23 times more than CO_2 does.[1] Thus, burning CH_4 would *de facto* reduce the greenhouse gases impact in the atmosphere, although at this stage of the game it is not a solution to global warming by itself.

The main problem with biogas resides in the fact that, in order to obtain a more profitable use of the methane, it is necessary to have it in its purest state, that is, without CO_2. However, both CH_4 and CO_2 are extremely stable molecules, which complicates their selective chemical separation, yet recent studies have proposed the use of bulk Transition Metal Carbides (TMCs) and their two-dimensional versions (MXenes) as materials capable of carrying out the separation of both molecules.[2,3]

Nowadays, membranes of porous materials have become potential candidates for the separation of molecules by taking advantage of the different diffusion energy for going across them. In this sense, two-dimensional (2D) carbon allotropes are materials with great prospective for their use as membranes. Studies with graphene nanostructures[4] or reduced graphene oxides[5] have proven to be good materials for biogas upgrading. Another interesting family of allotropes are graphynes,[6] structures that combine *sp* and sp^2 hybridizations of carbon atoms, different to the only sp^2 hybridization of graphene. These structures have been proposed in gas separation processes because, thanks to their versatility, allow designing their natural pores at will. In the last year, a new family of carbon allotrope structures have been presented, namely grazynes,[7] also built with *sp* and sp^2 carbon atoms hybridizations, and so, *de facto*, being graphynes. The difference raises in that grazynes combine different graphene stripes bonded to each other by acetylenic linkages, see Figure 1. As in graphynes, grazynes can be modified in different ways: Enlarging the acetylenic linkages length, the graphene stripes width, and having missing acetylenic linkages, which would increase the pore size. Therefore, grazynes can be postulated

as one of the most promising families of membranes for chemical resolution, here aimed at biogas upgrading, just thanks to the high tunability of the structure that allow creating pores rationally until the diffusion of one of the molecules present in the mixture across these pores is allowed.

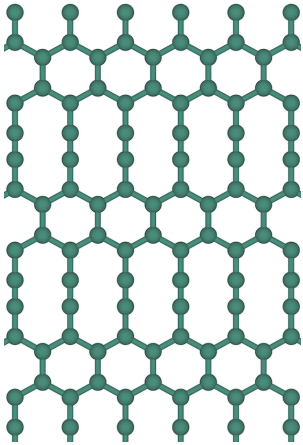

Figure 1: Top view of the [1],[1]-grazyne structure, this is, with its smallest graphene stripe and acetylenic linkage. Green spheres denote Carbon atoms.

In order to determine whether grazynes accomplish the requirements to perform the aforementioned process, one of the most efficient ways is to do it through computational estimations, nowadays normally tackled through Density Functional Theory (*DFT*) calculations, as done for other materials.[2,3] Through DFT one can determine the interactions between such materials surfaces and the molecules, as well as to seize the energy barriers of the diffusion through the pores. This information is useful to corroborate or discard the utility of the systems under study. Furthermore, one can acquire estimates of the diffusion rates, which can be useful to estimate the selectivities of the diffusion with respect the working temperature. Here, such an analysis is performed for both biogas molecules —CO_2 and CH_4— trespassing different grazyne structures, with the ultimate goal of finding structures capable of filtering any of the two molecules and thus, obtaining a purer methane stream.

4. OBJECTIVES

The main objective of this project is to find any grazyne structure capable to carry out the diffusion process of CO_2 or CH_4 and, therefore, to find a structure capable of being used as a filter to separate such molecules. To do so, adsorption and penetration barrier energies of different grazyne compounds are analysed by Density Functional Theory (*DFT*) means. The specific objectives of this work are:

- To evaluate the effect of coverage on the adsorption energies of CO_2 of CH_4 on three possible grazynes.
- To analyse the effect of the graphene width on the adsorption energies and diffusion energy barriers.
- To investigate the effect of dispersive forces on the CO_2 and CH_4 adsorption energies and diffusion energy barriers.
- To elucidate whether there is an effect of molecular conformation in the penetration process.
- To rationally design a membrane adequate for separating CO_2 form CH_4, *i.e.* applicable in biogas upgrading.
- To estimate the diffusion rate constants as a function of temperature to ascertain the filtering capabilities of such materials.
- To determine the selectivity of CO_2 over CH_4 in the structures where these adsorbates can go through its pores, to assess the biogas upgrading possibilities.

5. THEORY

5.1. SCHRÖDINGER EQUATION

Quantum chemistry is based on the principle that a system is completely described by a wavefunction, Ψ, at each instant of time. This function depends on the coordinates of the particles that form the system. The wavefunction does not represent any measurable property of the system, however, applying an operator to it, one can determine the value of a desired property. In this project, the total energy of the system, *E*, is needed to determine whether a suggested grazyne structure is suited for filtering CO_2 or CH_4 molecules. This energy can be determined by solving the time independent Schrödinger equation, where an operator called Hamiltonian, $\hat{H}$, acts onto the wavefunction, so that:

$$\hat{H}\,\Psi = \mathrm{E}\,\Psi \qquad \text{(Eq. 1).}$$

Having a system of *N* nuclei and *n* electrons, the Hamiltonian of the system would be:

$$\hat{H} = \hat{T}_e + \hat{T}_N + \hat{V}_{ee} + \hat{V}_{NN} + \hat{V}_{Ne} \qquad \text{(Eq. 2),}$$

where $\hat{T}_e$ represents the kinetic energy of electrons, $\hat{T}_N$ the kinetic energy of nuclei, and the potential repulsion between electrons, $\hat{V}_{ee}$, nuclei, $\hat{V}_{NN}$, and the potential attraction between nuclei and electrons, $\hat{V}_{Ne}$, is also accounted for.

To solve the Schrödinger equation (Eq. 1), it is useful to apply the Born-Oppenheimer approximation that allows decoupling the nuclear and electronic motion since nuclei are much heavier than electrons. Thus, by fixing the nuclear coordinates, it is possible to solve the electronic Hamiltonian with a reduced number of variables:

$$\hat{H}_{el} = \hat{T}_e + \hat{V}_{ee} + \hat{V}_{Ne} \qquad \text{(Eq. 3).}$$

Although the $\hat{V}_{Ne}$ term depends on nuclear and electronic coordinates, it does only parametrically on the nuclear coordinates so the electronic Hamiltonian operator, $\hat{H}_{el}$, depends only on the electronic coordinates. Thus, the equation to solve is the following:

$$\hat{H}_{el}\Psi = E_{el}\Psi \qquad \text{(Eq. 4).}$$

At this point, the mathematical complexity of the system has been reduced. However, the exact solution of Eq. (4) can be only obtained for really simple systems, *e.g.* hydrogen-like atoms. For more complex systems, N-electronic, such as those studied in this project, it is not possible to solve the Schrödinger equation, as one misses the correlation energy. Different approximated ab initio methods like Hartree-Fock (*HF*), Configuration Interactions (*CI*), or Møller-Plesset perturbational methods, *e.g.* MP2, have been developed, which allow us to get a good approximation of the electronic energy, but at a high computational cost. This is the reason why DFT methods are important as they represent a good compromise between computational cost and accuracy.

5.2. DENSITY FUNCTIONAL THEORY

DFT is one of the most widely used methods for solving the electronic structure of a given system. Thanks to its lower computational cost compared to other orbital based *ab initio* methods, it has become one of the most popular methods. The big difference among them is that DFT does not use the wavefunction, but uses the electronic density function instead. While the wavefunction of an *N* electron system depends on 3·*N* coordinates, 4·*N* if spin is accounted for, the electronic density function, $\rho(\mathrm{r})$, depends only on the three spatial variables, again four when considering spin. Clearly, this fact greatly simplifies the calculations. Although DFT use is widely extended, it was not until 1964 when Hohenberg and Kohn developed the theoretical basis of the method.[8,9]

Hohenberg and Kohn demonstrated that, for the ground state, there exists a relation between the electronic density and the external potential, $\mathrm{V_{ext}(r)}$. This means that the electronic density in the ground state has all the information of the electronic system. In their first theorem, Hohenberg and Kohn showed that the energy can be expressed as an energy functional using the relationship:

$$E[\rho] = F[\rho] + \int \rho(r) v_{Ne}(r) dr \qquad \text{(Eq. 5)},$$

where $F[\rho]$ represents the universal functional which includes the kinetic energy and the interaction between the electrons, and $v_{Ne}(r)$ is the interaction between the electrons and all the nuclei in a defined position.

With a second theorem, the authors demonstrated how the electronic density of the ground state is the one that minimizes the energy functional, $E[\rho]$, obtaining the ground state energy,

E_o. If the reader is curious and needs more details about these theorems, we recommend going to the bibliography where the most important ideas have been extracted from.[8,9]

5.2.1. Kohn-Sham Method

The Kohn-Sham method follows the Hohenberg-Kohn theorems, and describes a way to approximate the universal functional. To explain this, a fictitious system of electrons which do not interact with each other is used, which provides the same electron density of the real system under study. With all of this, the kinetic energy functional corresponds to a sum of two individual kinetic energies, one that can be exactly calculated and another which is a correction term that contributes in a small quantity to the total energy, so that in a short notation;

$$E = T_s + E_{ext} + J + E_{xc} \qquad \text{(Eq. 6)},$$

where T_s is the kinetic energy of the electrons of the system, E_{ext} corresponds to the attraction between the external potential and the electron density, J represents the coulombic repulsion between electrons, and E_{xc} is the exchange-correlation functional, that corresponds to the difference between the non-interacting electrons system and the real system. The E_{xc} term has no exact definition, but there are different good approximations for estimating it, briefly explained next.

5.2.2. Exchange and Correlation Functionals

As aforementioned, when using DFT method it is important to know how to approximate the E_{xc} contribution. Nowadays, the exact value of the exchange-correlation (*xc*) functional has not been defined yet. However, it has been studied for many years and there exist some different ways to get an approximated result. Five different manners to get the expression are sorted from the simplest way to the most complex one, see Figure 2, according to the Jacob's Ladder of *xc* functional development.[10]

The first approximation and most basic level is known as the Local Density Approximation (*LDA*), which hypothesizes that the electronic density only depends on the spatial coordinates. The second level is the Generalized Gradient Approximations (*GGA*), where the functional depends on the electron density *and* on the electron density derivative. This level is the chosen one for this project, particularly using the Perdew-Burke-Ernzerhof (*PBE*) *xc* functional,[11] as such

a functional duly describes the energetics of carbon allotropes. The third level is the meta-GGA functionals, which also include the second density gradient, *i.e.*, the kinetic energy density. The last levels are more loosely defined, but normally the fourth belongs to hybrids methods where *xc* functionals combine some LDA and/or GGA contributions with some portion of the HF exchange energy. The hybrid *xc* functionals considers the occupied orbitals whereas the double hybrid functionals take into account the virtual orbitals, and could be considered as a fifth rung of the ladder.

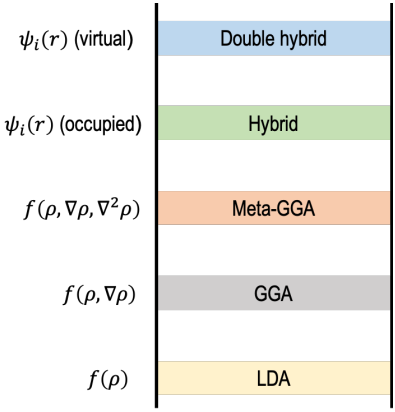

Figure 2: Representation of the different xc functionals for DFT within the so-called Jacob's Ladder of improvement.

5.3. CARBON ALLOTROPES

The tetra-valence of carbon atoms make them capable to form many different structures with many different forms and properties. Many of them are well-known, such as diamond or graphite, but there are some other allotropes less known with excellent properties and that concentrate lots of scientific attention. This section aims at introducing the reader to the different types of carbon allotropes, especially those related to the project.

5.3.1. Diamond

Diamond is, surely, the best-known carbon material thanks to its extreme hardness and beauty. It consists in a network of sp^3 hybridized carbon atoms linked by σ-type bonds. The unit cell is shown in Figure 3 and it is a variant of a face-centred cubic (*fcc*) structure called diamond lattice. In this structure, the carbon atoms are located at the vertices of the cube, the centre of the faces and in half of the tetrahedral sites. The peculiarity of this material is that each atom is covalently

linked with four other carbon atoms, making a very compact packing. Its hardness, one of the great features of diamond, is a consequence of this dense packing. Apart from its robustness and its peculiar visual appearance, diamond also stands out for its high melting and boiling points, for its high insolubility, and for being a natural insulator.

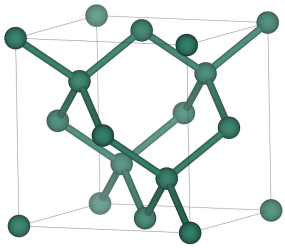

Figure 3: Representation of the diamond unit cell. A *fcc* structure with half of the tetrahedral sites occupied. Carbon atoms are shown as green spheres.

5.3.2. Graphite

The main difference between diamond and graphite is how carbon atoms are bonded, which in turn delivers totally different properties. Graphite is composed of flat layers of carbon atoms with sp^2 hybridization, see Figure 4, forming hexagonal structures, where each atom is bonded to other three neighbouring carbon atoms. Such graphite layers are bonded in between through dispersive forces, such as van der Waals (vdW) interactions. Within a layer, the delocalized structure of the π electrons reduces the bond lengths, actually being shorter than in diamond. The delocalized structure of free electrons is the reason why graphite is a great electrical conductor, while the interlayer vdW interactions confer softness to graphite, being easy to exfoliate, giving the possibility of having pencil leads out of graphite, or using it as a dry lubricant.

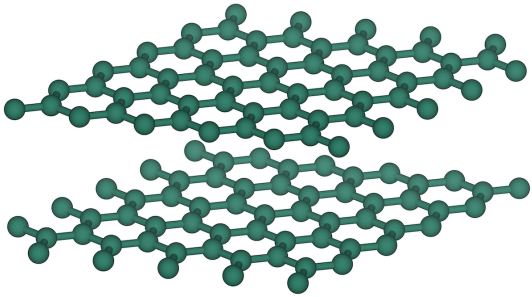

Figure 4: Top view of graphite structure. Carbon atoms are shown as green spheres.

5.3.3. Graphene

Since 2004, when graphene was characterized for the first time by Geim and Novoselov,[12] the research about this compound has increased significantly. Graphene is, simply, a single layer of graphite, and so made of hexagonal displays of sp^2 hybridized carbon atoms, see Figure 5. As aforementioned, the extremely tight packing of atoms in the crystal lattice makes graphene a highly stable compound, with outstanding capabilities in terms of charge transport.[13] Aside, graphene possesses a wide range of other beneficial properties, including as a high degree of flexibility, a high mechanical strength, and optical transparency. These properties depend on the numbers of graphene layers, as in few-layered graphene,[12] and also on the defects present in the structure, such as in nonporous graphene.[14] These characteristics made graphene a compound with a wide range of applications, and the starting point to other materials that are fully or partially hydrogenated, such as graphane,[15] or graphone.[16]

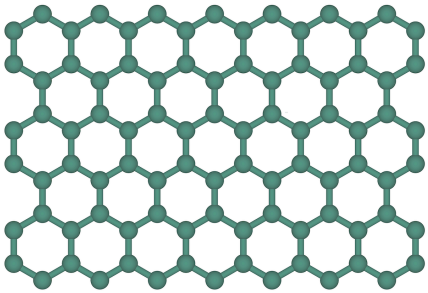

Figure 5: Top view of graphene. Carbon atoms are shown as green spheres.

5.3.4. Graphynes

It was already in 1987 when Baughman *et al.* proposed the family of graphynes.[17] The structure of graphyne consists of a 2D network of hexagonal carbon rings, with sp^2 hybridization, linked by acetylenic bonds, with *sp* hybridizations, see Figure 6. Although this new material allows to create different graphyne compounds, which are less stable than graphene because acetylenic bonds reduce the cohesive energy.[6] The properties of the material depend on its structure, but, in general, recent studies indicate that graphynes may transport charge even faster than graphene,[18] and with anisotropy depending on the graphyne structure. Mechanical properties are a bit different than in graphene because when having *sp* carbon atoms one reduce the flexibility of the layer, and thus, the rigidity increases, making it a brittle material.[19]

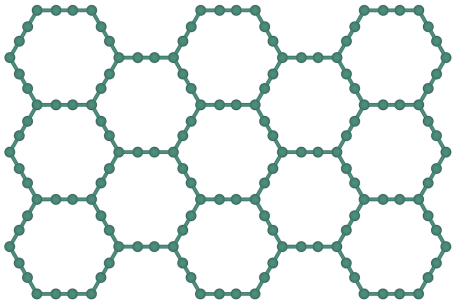

Figure 6: Top view of a graphyne structure. Carbon atoms are shown as green spheres.

5.3.5. Grazynes

Grazynes are based on graphynes, and are composed of graphene stripes linked together through acetylenic linkages.[7] Thus, they display sp^2 and *sp* carbons, see Figure 7. One can modify the linkages length and the graphene stripes to get a wide variety of compounds, this together with the possibility of having alternate graphene stripe widths, and alternate acetylenic lengths, as well as having defects like missing acetylenic linkages. In this work, we focus on the biogas filtering of grazynes, so we will exploit these tuning capabilities to design grazynes tailor-made for such a purpose.

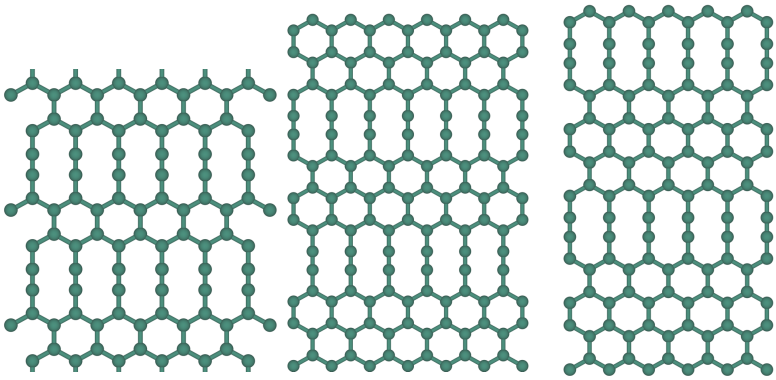

Figure 7: [1],[1]-grazyne (left), [2],[1]-grazyne (middle), and [3],[1]-grazyne (right), all varying in the graphene stripe width. Carbon atoms are shown as green spheres.

5.4. UNIT CELLS

As above shown, the studied structures display an intrinsic periodicity so they can be described using a unit cell. For crystalline bulk structures, the unit cell is the most basic repeating structure where all atoms are ordered following the same pattern. The primitive unit cell corresponds to the lowest volume unit cell repeated through the crystalline structure, and the network created by the unit cell repetition is called the lattice. Any unit cell is defined by three vectors (**a**, **b**, **c**) and three angles (α, β, γ), see, *e.g.*, a body centred tetragonal cubic cell with modules $a = c \neq b$ and $\alpha = \beta = \gamma = 90^{o}$ in Figure 8.

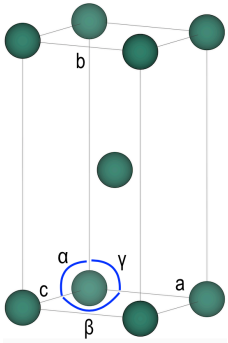

Figure 8: View of a body centred tetragonal unit cell. Colour code as in Figure 7.

5.4.1. Reciprocal Space

The Bloch theorem for crystal systems indicates that, applying translational symmetry to the unit cell, the wavefunction that solves the Schrödinger equation must be periodic as well, and takes

the form of two different functions, the first one contains the periodicity term and the second one is a planewave. The wavefunction is actually a summation of planewaves defined in the reciprocal space, which allows describing the system only using a single unit cell.

The reciprocal space is the Fourier transform of the real space, and is defined by cell vectors ($\mathbf{a}^*, \mathbf{b}^*, \mathbf{c}^*$) which are related to the vectors of the real cell ($\mathbf{a}, \mathbf{b}, \mathbf{c}$) by the following relation:

$$\mathbf{a}^* = 2\pi \frac{\mathbf{b}\times\mathbf{c}}{\mathbf{a}\cdot(\mathbf{b}\times\mathbf{c})}; \quad \mathbf{b}^* = 2\pi \frac{\mathbf{c}\times\mathbf{a}}{\mathbf{b}\cdot(\mathbf{c}\times\mathbf{a})}; \quad \mathbf{c}^* = 2\pi \frac{\mathbf{a}\times\mathbf{b}}{\mathbf{c}\cdot(\mathbf{a}\times\mathbf{b})} \qquad \text{(Eq. 7)},$$

where, looking at the inversely proportion between the reciprocal and the real vectors, the larger the direct cell is, the smaller is the reciprocal cell one, and *vice versa*.

In this sense, DFT calculations of crystal systems need to perform many non-easy volume integrals associated to the reciprocal space of the unit cell, also called **k**-space. To solve this problem, the integration over the entire volume is approximated to a summation over particular points on the unit cell. These points are the **k**-points, and they are normally defined through a mesh of equally spaced points. A better description of the system is obtained including a higher number of **k**-points although once the energy is converged a further increase in the number of **k**-points does not report more accuracy to the calculation, yet only increases the computational cost. As above stated, the larger the real cell is in one direction, the smaller it is in the reciprocal space, and fewer **k**-points are needed in that direction.

5.4.2. Slab Model

In nature, crystals are three-dimensional objects terminated by surfaces. It is on these surfaces where many phenomena and processes occur, so modelling surfaces is of great practical and theoretical interest. To study a periodic surface it is important to use a model which would allow assessing the energy associated to the surface formation and its relaxation. The slab model is a periodic model used for the study of periodic surfaces within Periodic Boundary Conditions (*PBC*). The slab model consists on different atomic layers stacked along the modelled surface, where normally one or more bottom layers are kept fixed to simulate the material bulk behaviour. The other layers are allowed to relax in all three directions for effectively modelling the surface.

At variance to such models, the present materials, grazynes, feature only one atom thick layers. However, different approaches have been used on this study accounting for relaxation. First, we have fixed all atoms, simulating a rigid solid. In a second approach, a single atom of the structure is fixed, allowing the mobility of all the other atoms. This anchor atom is used to avoid displacements of the full grazyne layer. Finally, notice that PBC go along all directions; thus, to avoid interactions with other atoms perpendicular to the structure under study, a vacuum zone is added above and below the monolayer, see Figure 9. Normally, 10 Å of total vacuum avoids any type of interaction with translationally repeated slabs.

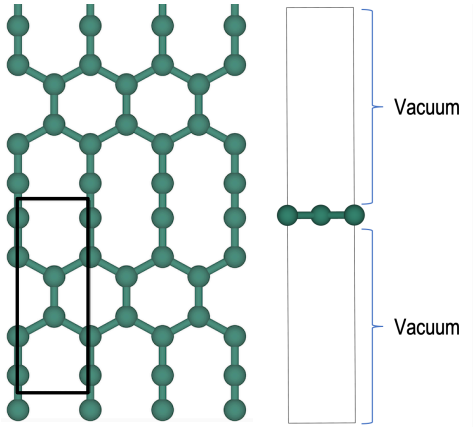

Figure 9: Top (left) and side (right) views of [1],[1]-grazyne. Unit cell is shown in black. Colour code as in Figure 7.

5.4.3 Supercells

When studying adsorption processes on a periodic surface, it is necessary to consider the possible interactions that can occur between adsorbates located close to each other. To study the process in a clean way it is important to minimize these interactions. In the study carried out in this project, it is important to study situations where CO_2 and CH_4 do not have unwanted nearby interactions, so to obtain more satisfactory results. Even in the study of a single molecule adsorbing on the periodic cell, such periodicity and the interactions between molecules with the same translational image must be taken into consideration. To minimize these interactions, so-called supercells are used, these are, cells that have been enlarged, *i.e.*, multiplied a certain number of times from the basic unit cell. This new cell effectively increases the distance between adsorbates, decreasing such interactions as above mentioned. Figure 10 shows the difference in

coverage between the smallest unit cell (left) and a (2×2) supercell (right). It is easily noticeable that the distance between adsorbates is larger in the supercell, *i.e.*, the coverage is reduced, thus, reducing the interaction between the adsorbates. However, the computational cost associated to the supercell description obviously increases.

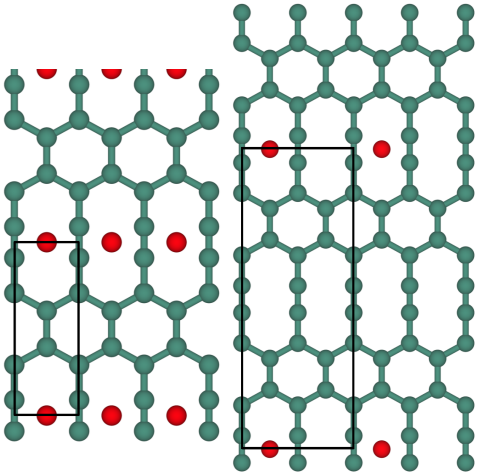

Figure 10: Comparison of the basic unit cell (left) and a c(2×2) supercell (right) on [1],[1]-grazyne. The unit cell of each structure is shown in black. Carbon atoms of the grazyne structure are colored in green, while red spheres denote O atoms for a perpendicular adsorption of CO_2 molecules.

5.5. ADSORPTION

Adsorption is the process by which atoms and molecules —adsorbates— interact with a surface —substrate—. It is important not to mix adsorption with absorption, as the latter implies the atom or molecule getting inside the substrate lattice. There are two types of adsorptions depending on the interaction strength between adsorbate and substrate: physisorption and chemisorption. Physisorption occurs when the interaction is weak, and this normally results from dispersive forces, such as van der Waals interactions. An important fact about the physisorption is that the molecular shape of the adsorbate does not change much during the process. The physical adsorption is not specific of a site and so can take place all over the surface. In the chemisorption the interaction is strong and the molecule can get very distorted, normally due to the formation of a new bond. Chemisorption is highly specific on particular adsorption sites. To determine whether an adsorption is weak or strong one can seize it through the adsorption energy, E_{ads}. The adsorption energy can be determined as:

$$E_{ads} = E_{S/A} - E_S - E_A \quad \text{(Eq. 8)},$$

where $E_{S/A}$ is the energy with the atom or molecule adsorbed on the substrate, E_S represents the substrate energy, and E_A is the energy of the adsorbate in vacuum. Within this definition a negative value of adsorption energy indicates a stabilization of the adsorbate over the surface, whereas a positive value indicates that both species are more stable separated than interacting. Along this line, the more negative the $E_{S/A}$, the stronger the adsorption.

5.5.1. Penetration Barriers

In order to find structures capable to act as a filter to separate CO_2 and CH_4 molecules, it is necessary that the energy barrier between the Transition State (*TS*), *i.e.*, the point where the molecule is just trespassing the material pore, and the state with the adsorbed molecule is as small as possible, yet significantly different for each molecule, see Figure 11.

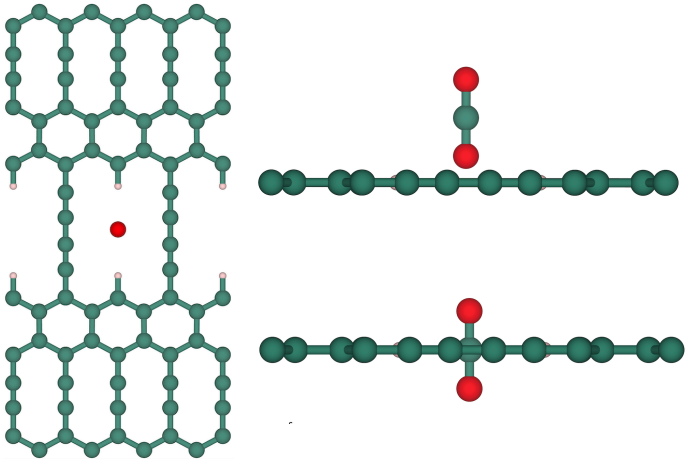

Figure 11: Top view of [1],[1,2]{0,1}-grazyne hole (left), and side views of the adsorbed (right top) and transition states (right bottom). Carbon, Oxygen, and Hydrogen atoms are shown as green, red, and white spheres, respectively.

Once the energies of both systems have been determined, and knowing that the TS and the adsorbed state correspond both to stationary points of the potential energy surface, it is possible to estimate the energy barrier, E_b, as:

$$E_b = E_{TS} - E_{S/A} \quad \text{(Eq. 9)},$$

where E_{TS} is the transition state energy.

5.5.2. Diffusion Rates

As shown by the Arrhenius equation, the rate constant of a reaction or a process, *k*, depends on the activation energy and the temperature:

$$k = Ae^{-\frac{E_a}{RT}} \quad \text{(Eq. 10)},$$

where A is the pre-exponential factor, E_a the activation energy, *T* the absolute temperature, and R the gases constant. The Arrhenius equation can be used to determine the effect of the temperature on the rate constant. It is possible to calculate the penetration rate constants for both CH_4 and CO_2 molecules by first principles, using statistical thermodynamics through the general expression for the rate constant of a process:

$$k = \frac{k_B T}{h}\frac{q^{\neq}}{q_r}e^{-\frac{\Delta E^{\neq}}{k_B T}} \quad \text{(Eq. 11)},$$

where k_B is the Boltzmann constant and h the Planck constant. The $q^{\neq}$ and q_r terms stand for the partition function of the TS and of reactants, respectively, where here it would imply the adsorbed molecule. To understand this contribution into the rate constant it is important to know that the overall partition function for a gas molecule is a product of the respective partition functions of vibrations, rotations, translations, and electronic configurations:

$$q = q_{vib} \cdot q_{rot} \cdot q_{trans} \cdot q_{elec} \quad \text{(Eq. 12)}.$$

Nevertheless, only the vibrational partition function takes part on the rate constant equation because for adsorbed species rotational and translational modes become frustrated by the substrate presence and the formed bond in the adsorption. In reference to the electronic part it is important to note that the difference between the ground state and the excited states is normally high, so the electronic partition function can be taken as one. Thus, only the vibrational partition function is needed, and it can be calculated as:

$$q_{vib} = \prod_i \frac{1}{1-e^{-\left(\frac{h\nu_i}{k_b T}\right)}} \quad \text{(Eq. 13)}.$$

The vibrational frequencies, ν_i, are calculated by DFT by the Hessian matrix construction and diagonalization by finite displacements. This would render 3N-6 frequencies for CH_4 and 3N-5 for CO_2, being N de number of atoms of the molecule. When each molecule adsorbs a total of 3N normal modes of vibration are obtained, due to translations and rotations frustrated movements. When the stationary point corresponds to a local minimum all the normal modes frequencies are real. In the case that one of the normal modes has an imaginary frequency the stationary point corresponds to a TS. In the case of membranes, the imaginary vibrational frequency corresponds to the movement across the membrane since it is essentially the barrier needed to surmount to pass from one side to another side of the membrane. By knowing the diffusion rates, it is possible to estimate the selectivity of CO_2 over CH_4,[3] defined as;

$$S_{CO_2/CH_4} = \frac{K_{CO_2}}{K_{CH_4}} = \frac{e^{-\Delta E_{ads}^{CO_2}/k_B T}}{e^{-\Delta E_{ads}^{CH_4}/k_B T}} \quad \text{(Eq. 14).}$$

6. COMPUTATIONAL DETAILS

Present DFT calculations have been done using the Vienna *Ab Initio* Simulation Package (*VASP*),[20] employing Projected Augmented Wave (*PAW*) pseudopotentials to treat core electrons,[21] while valence electrons have been described using a planewave basis set of 415 eV of kinetic energy cutoff. Calculations have been carried out using the PBE *xc* functional,[11] but also including the Grimme D3 description of dispersive forces (PBE-D3).[22] The CH_4 and CO_2 molecules were calculated by using one single **k**-point inside a unit cell of 10×10×10 Å. The electronic and ionic convergence criteria were set to 10^{-6} and 10^{-5} eV, respectively.

Three different grazynes were initially considered; these are, [1],[1]-grazyne, [2],[1]-grazyne, and [3],[1]-grazyne, see Figure 6. Larger *c*(2×2) supercells were built from them, including defective sites, where dangling covalent bonds have been capped with H atoms. Optimal Monkhorst-Pack **k**-points grids were used for the different unit cells, following the work of Kamalinahad *et al.*,[7] being 20×20×1, 17×13×1, and 19×19×1 for [1],[1]-, [2],[1]-, and [3],[1]-grazynes, respectively. A vacuum of 10 Å was always added up and down and perpendicularly to the surface to prevent any interaction between translational repeated slabs. This level of calculation was found to deliver energies converged below the chemical accuracy, usually set to 1 kcal·mol^{-1}, *ca.* 0.04 eV.[7]

Test calculations were carried out using a rigid solid, a completely relaxed solid, and an intermediate situation where a grazyne C atom is kept fixed so to avoid material drifting. However, no large differences were found among the different options, so the results discussed in the following have been gained with only one fixed C atom in all the structure. Different insertion modes have been studied for CO_2 and CH_4 molecules, *e.g.* being CO_2 perpendicular or parallel to the grazyne plane, or having three or one H atoms of CH_4 pointing towards the grazyne layer. Adsorption minima and TSs have been characterized as so by a frequency analysis, obtained through finite displacements of 0.03 Å length.

7. RESULTS AND DISCUSSION

7.1. INITIAL EXPLORATION

In order to find structures capable of acting as filters for the CO_2 and CH_4 molecules, different grazyne structures have been studied, which vary in the size of the acetylenic pores. In this sense, the project began with the study of the [1],[1]-grazyne, [2],[1]-grazyne, and [3],[1]-grazyne structures, see Figure 6, where the pore size is the smallest possible. Notice that the three structures have similar acetylenic pores, and differ basically on the graphene stripe width. As explained below, after obtaining the results of these systems, and viewing the impossibility of CO_2 and CH_4 molecules to diffuse across the membrane, the structures were modified using first supercells and subsequently enlarging the acetylenic pores.

7.1.1. CO_2 Diffusion

For the CO_2 penetration, two possible molecular orientations were considered; either with the molecular axis being perpendicular or parallel to the grazyne plane. Initially, the molecule was placed over the centre of the acetylenic pore, *ca.* 2 Å above, and let relax, *i.e.* to adsorb. In the case of the parallel adsorption, the molecular axis was parallel to the acetylenic connections. The PBE and PBE-D3 adsorption energies, E_{ads}, are listed in Table 1. Furthermore, the molecule was artificially placed in the centre of the pore, and let relax. Such a resulting energy was used to get a first, gross estimate of the penetration energy barriers, E_b, encompassed as well in Table 1.

One could inspect these first results having in mind that a suited diffusion process should display moderate energy barriers, normally below 1 eV. At the same time, it would be valuable to feature low adsorption energies, ideally belonging to physisorption, as large E_{ads} values would imply that the material would capture the molecules, rather than acting as a filtering membrane. The values listed in Table 1 clearly show that none of grazynes could allow the CO_2 trespassing, with PBE E_b values ranging 10.4 to 11.3 eV. Furthermore, the adsorption energies are positive, from *ca.* 0.5 to 0.7 eV. In other cases of Table 1, no barrier could be estimated, as the structure collapsed or evolved to other unstable structures.

Cell	Grazyne	PBE				PBE-D3			
		Perp.		Paral.		Perp.		Paral.	
		E_{ads}	E_b	E_{ads}	E_b	E_{ads}	E_b	E_{ads}	E_b
***c*(1×1)**	**[1],[1]**	0.58	11.24	0.57	—	0.47	11.12	0.47	—
	[2],[1]	0.62	10.48	0.62	—	0.52	10.38	0.41	—
	[3],[1]	0.66	10.69	0.65	—	0.54	10.59	0.43	—
***c*(2×2)**	**[1],[1]**	0.01	—	0.00	—	-0.22	—	-0.36	—
	[2],[1]	0.01	—	0.00	—	-0.07	—	-0.05	—
	[3],[1]	0.01	—	-0.29	—	-0.08	—	-0.19	—
***c*(2×2)**	**[1],[1,1]{0,1}**	0.00	6.72	0.05	16.70	-0.05	6.53	0.00	16.60

Table 1: Adsorption, E_{ads}, and penetration energy barriers, E_b, of CO_2, as estimated for different grazyne membrane models. All values are given in eV.

Thus, it seems clear that there are lateral steric repulsions on the *c*(1×1) models, and that the pore size is too small. Furthermore, the PBE-D3 results are very similar to the PBE ones, thus reducing E_{ads} and E_b by at most 0.12 eV. Given the large energy barriers and the steric repulsions, *c*(2×2) supercells were modelled, and, as seen in Table 1, the effect on the adsorption energies is quite significant, with reductions of up to 0.83 eV as observed for [1],[1]-grazyne. Generally, the adsorption energies are quite moderate, around zero as obtained at PBE level, and just slightly negative at PBE-D3 level, with no clear preference for the perpendicular or parallel adsorption, characteristic of a physisorption. Notice that there are structures which do not feature an E_b value, simply because in the course of the optimization within the hole, the system breaks down or evolves to other unstable structures given the high repulsion among the atoms; for instance, see the case of *c*(2×2) [2],[1]-grazyne in Figure 12. There, the CO_2 was placed just in the middle of the acetylenic hole and the high repulsion between molecule and grazyne perturbs the full grazyne structure, resulting in a reorganization of the structure forming stripes of five and seven atoms rings, the so-called Stone-Wales defects.[23] This is probably due to the point that the acetylenic hole is still too small.

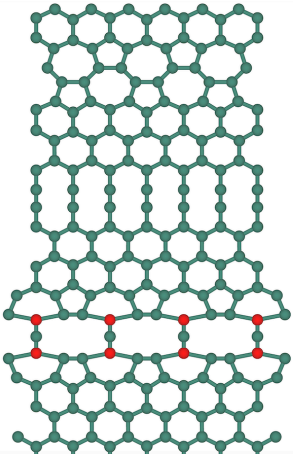

Figure 12: Final structure of [2],[1]-grazyne c(2×2) obtained from locating one CO_2 molecule just in the middle of the acetylenic pores. Carbon and Oxygen atoms are coloured as green and red spheres, respectively.

To solve that, one can subtract two C atoms of every second acetylenic linkage, of every second acetylenic stripe. This is achieved in the [1],[1,1]{0,1}-grazyne, see Figure 13. As seen in Table 1, the E_{ads} values are close to zero, indeed ±0.05 eV. Furthermore, the energy barriers are clearly reduced, particularly for the perpendicular CO_2, reaching values of 6.72 and 6.53 eV at PBE and PBE-D3 levels, respectively. These values mean a reduction of more than 4.5 eV compared to equivalent conformations as found on the [1],[1]-grazyne model. Furthermore, as seen in Figure 13, the TS does not perturb the material structure.

Despite the above comments, after studying these different types of structures and seeing the obtained energy values, it is clear that the diffusion process of CO_2 is unlikely to take place on such models, since the energy barriers are still too high. However, this first screening served to see that the energy barrier decreases while the acetylene pore lengthens, which opens the possibility to reach suited values when one would continue enlarging. However, the employed models were large enough so as to display slightly negative adsorption energies, which is a good indicator that such layers could be used as membranes for filtering molecules.

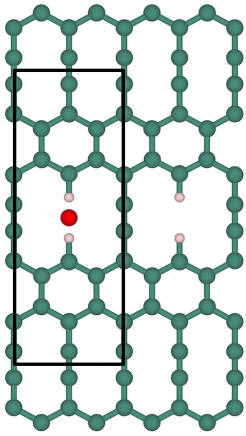

Figure 13: Top view of the TS for CO_2 perpendicular diffusion on [1],[1,1]{0,1}-grazyne structure. Carbon, Oxygen, and Hydrogen atoms are shown as green, red, and white spheres, respectively.

7.1.2. CH_4 Diffusion

As done before for CO_2, the CH_4 adsorption and penetration has been calculated in two different positions with one C-H bond perpendicular to the grazyne surface; one case with the hydrogen bond pointing down towards the grazyne layer, and the other one pointing up, towards the vacuum. The same grazyne models used for CO_2 have been also inspected, and the obtained results are listed in Table 2.

Cell	Grazyne	PBE				PBE-D3			
		Down		Up		Down		Up	
		E_{ads}	E_b	E_{ads}	E_b	E_{ads}	E_b	E_{ads}	E_b
***c*(1×1)**	**[1],[1]**	1.12	—	1.12	—	1.40	—	0.96	—
	[2],[1]	1.21	—	1.22	—	1.05	—	1.06	—
	[3],[1]	1.27	—	1.27	—	1.11	—	1.10	—
***c*(2×2)**	**[1],[1]**	-0.11	—	-0.16	—	-0.30	—	-0.30	—
	[2],[1]	-0.08	—	-0.01	—	-0.22	—	-0.15	—
	[3],[1]	-0.14	—	-0.05	—	-0.25	—	-0.21	—
***c*(2×2)**	**[1],[1,1]{0,1}**	-0.01	—	-0.01	—	-0.12	—	-0.16	—

Table 2: CH_4 adsorption and barrier energies on the studied grazyne models. All values are given in eV.

Knowing that the CH_4 molecule has a somewhat larger size compared to CO_2, one expects getting larger energy barriers, as shown in Table 2. The E_{ads} values are larger, generally above 1 eV for the *c*(1×1) cells. Furthermore, when trying to localize the diffusion TS, big distortions are encountered, being the reason why the dashed lines in Table 2; see for instance the *c*(1×1) of [3],[1]-grazyne in Figure 14, where the CH_4 molecule is broken and fragments incorporated to the grazyne lattice, converting the acetylenic linkages in five-rings chains, aside from having hydrogenated C atoms and the formation of a H_2 molecule. Again, the effect of vdW forces affects the adsorption energies by 0.28 eV at most, being thus a small contribution. By using *c*(2×2) supercells the high repulsions between methane molecules disappear, showing moderate adsorption energies ranging -0.01 to -0.30 eV, thus being physisorption processes. The same applies on the defective *c*(2×2) [1],[1,1]{0,1}-grazyne model.

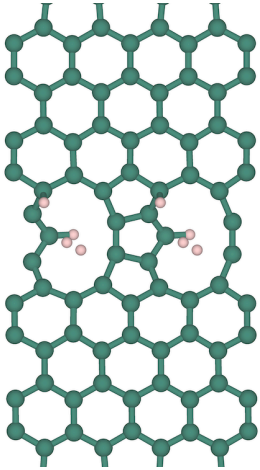

Figure 14: Top view of the c(2×2) supercell of [3],[1]-grazyne after placing one CH_4 molecule in the acetylenic hole. Colour coding as in Figure 13.

7.2. OPTIMAL STRUCTURES

After the study of all previous grazynes, three different ones were created adding an extra acetylenic bond to the [1],[1,1]{0,1}-grazyne, [2],[1,1]{0,1}-grazyne and [3],[1,1]{0,1}-grazyne, *i.e.*, [1],[1,2]{0,1}-, [2],[1,2]{0,1}-, and [3],[1,2]{0,1}-grazyne, respectively. An example of these new C-based membranes is shown in Figure 15, and it is important to note that the new length of acetylenic linkages makes holes bigger. As in the other cases, the diffusion process of CO_2 and CH_4 were studied in these new structures.

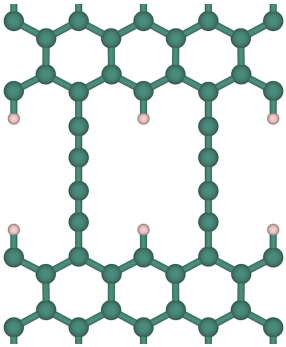

Figure 15: Top view of [1],[1,2]{0,1}-grazyne. Colour coding as in Figure 13.

7.2.1. CO_2 Diffusion

As above mentioned, two possible orientations of CO_2 were considered; perpendicular or parallel to the grazyne plane. The TS estimation process was the same as for the other structures, initially placing the molecule 5 Å above the grazyne and then approaching the molecule until located just in the middle of the pore. E_{ads} are shown in Table 3, as well as E_b.

Grazyne	PBE				PBE-D3			
	Perp.		Paral.		Perp.		Paral.	
	E_{ads}	E_b	E_{ads}	E_b	E_{ads}	E_b	E_{ads}	E_b
[1],[1,2]{0,1}	0.01	0.79	0.04	8.51	-0.04	0.56	0.00	8.38
[2],[1,2]{0,1}	0.01	0.86	0.05	8.78	-0.03	0.63	0.01	13.27
[3],[1,2]{0,1}	0.01	0.89	0.06	13.82	-0.03	0.66	0.02	13.71

Table 3: Adsorption, E_{ads}, and penetration energy barriers, E_b, of CO_2, as estimated for different grazyne c(2×2) membrane models. All values are given in eV.

The adsorption energies obtained are relatively low when compared with the energies shown in Table 1. These energies show that the pore size can be adequate for the CO_2 diffusion process. Observing Table 1, it can be seen how the values for PBE-D3 are slightly lower than the values obtained for PBE, even becoming negative for CO_2 perpendicular to the plane. This negative energy suggests that there is a process of attraction between substrate and adsorbate. In addition, the E_b obtained are less than 1 eV, which means that the barrier is low enough for the CO_2 to pass across the grazyne surface and, thus, to be able to penetrate the entire structure. On the other hand, it should be noted that, although the adsorption energies between

perpendicular and parallel CO_2 are similar, is not the same for penetration energy barriers, the latter being very high for parallel CO_2. This is due to the fact that the interactions with the grazyne are greater at the TS, thus increasing the E_b. It is clear that the parallel CO_2 diffusion process could not be carried out through this conformation. Furthermore, the CO_2 structure in TS was modified during calculations, going from being a linear molecule to a molecule with an angle of 102º, see Figure 16. Most likely, the double bonds in the molecule were broken, and bonds were formed between adsorbate and grazyne.

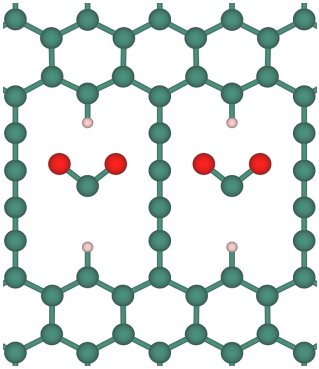

Figure 16: Transition state of [1],[2]{1}-grazyne. Note that CO_2 does not have a lineal form. Carbon, Oxygen, and Hydrogen atoms are shown as green, red, and white spheres, respectively.

7.2.1.1. Penetration Barrier Study

Viewing that these new structures seem to be capable to act as a CO_2 filter, a more exhaustive study of the energy barrier have been carried out. In this way, the energetic profile of these systems has been studied placing the CO_2 at different distances from the surface of the grazyne, starting at a distance of 5 Å and ending at 0.1 Å. Moreover, and to be sure that the adsorbate does not change, the position of the CO_2 carbon atom has been fixed, so that the CO_2 cannot move in full and reach during the optimization the adsorption sites minima.

The different obtained energy profiles reveal that E_{ads} increases as the adsorbate approaches the pore, being the TS the most energetic point, as expected. As shown in Table 3, E_b values are still low and the diffusion process appears feasible in the three types of grazynes. With these values it is possible to draw the reaction coordinate, see Figure 17. From it, it is clear that PBE provides higher E_{ads} values compared to PBE-D3, by *ca.* 0.15 eV.

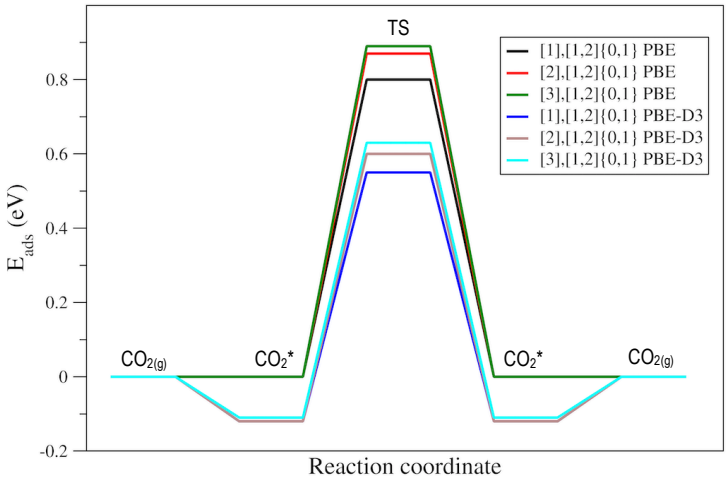

Figure 17: Diffusion across grazyne energy profile for perpendicular CO_2. TS represents the transition state and CO_2* the adsorbed state.

On the other hand, the study for parallel CO_2 has also been carried out, obtaining different results. The process followed is the same, initially placing the adsorbate at 5 Å and decreasing the distance to the grazyne until 0.1 Å. Table 4 compiles all the described energies.

	PBE			**PBE-D3**		
h	**Parallel**					
	[1],[1,2] {0,1}	**[2],[1,2] {0,1}**	**[3],[1,2] {0,1}**	**[1],[1,2] {0,1}**	**[2],[1,2] {0,1}**	**[3],[1,2] {0,1}**
5	0.04	0.05	0.06	0.00	0.01	0.02
4	-0.82	0.05	0.06	-0.04	-0.02	-0.01
3	-0.87	0.06	0.08	-0.09	-0.06	-0.05
2	-0.79	0.17	0.21	-0.02	-0.01	0.03
1.5	-0.65	0.29	0.37	0.14	0.09	0.16
1	-0.38	0.47	0.49	0.40	0.30	0.29
0.7	-0.17	0.67	0.58	0.52	0.38	0.43
0.4	0.09	0.95	0.87	0.87	0.76	0.71
0.1	0.12	0.72	0.78	0.89	0.49	0.58

Table 4: Adsorption energies, E_{ads}, for parallel CO_2 at different distances of grazyne. Distances are given in Å and energies in eV.

At first sight, parallel CO_2 trespassing results are a bit surprising as values do not follow the same trend as for the CO_2 perpendicular cases, being, in general, the TS well-passed the membrane layer. The explanation for this is that, as the molecule gets closer to grazyne, the latter bulges away from the adsorbate, creating asymmetries in the penetration profile, making the estimate of the height, *h*, somewhat unrealistic. See for instance an example of this bulging phenomenon in Figure 18 for the [2],[2]{1}-grazyne case. This fact indicates that the size of the pore is not large enough for the parallel CO_2 molecule to pass across, forces the membrane to bulge out, as a way to create more space in the hole for the molecule to go through. For instance, in the case shown in Figure 18, the CO_2 was initially placed 0.1 Å away from the membrane surface, but, after the calculation, the grazyne pore moved 2.3 Å away from the molecule getting a more stable system.

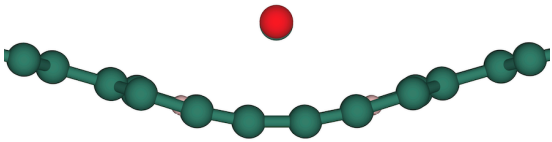

Figure 18: Adsorption process of parallel CO_2 at [2],[2]{1}-grazyne, firstly placed at 0.1 Å of distance. Carbons and Oxygen are represented as green or red spheres, respectively.

With these values at hand a few primary conclusions can be extracted. The adsorption and the penetration barriers energies obtained for the perpendicular CO_2 allow one thinking that the diffusion process for this molecule is likely to happen, given the moderate E_{ads} and E_b values. The most important fact is actually that the penetration barriers are below 1 eV, obviously feasible when enlarging the acetylenic bonds.

From the above, the distinct behavior of parallel CO_2 compared to perpendicular CO_2 is evident: First, notice the modification of the linear structure of parallel CO_2, as seen in Figure 16, and the extremely high E_b for parallel CO_2, as seen from Table 3. From the grazyne bulging and distancing from the CO_2 it is clear that parallel CO_2 will not be able to pass through acetylenic pores, at least on the studied compounds. In conclusion, the diffusion process will be only possible from a perpendicular CO_2 conformation, which, despite being feasible, would be prevented from a rapid diffusion as the process would be biased on how the CO_2 dynamically reaches the grazyne pore in a perpendicular fashion.

7.2.2. CH_4 Diffusion

As above done for the other CH_4 systems, the adsorption and penetration have been calculated in two different methane positions; one case with the hydrogen pointing down towards the grazyne, and the other case pointing up towards the vacuum. The same grazyne compounds as in previous section have been studied, and the resulting values are listed in Table 6. As occurred with CO_2 results, the adsorption energy values obtained for these systems are low and some of them are negative, however, these values are near 0 eV, so the attraction process will be very weak. The most important thing that can be extracted from Table 5 is that the systems resulting from the calculations of TS show how the methane molecules are repelled away from the surface, see Figure 19.

Grazyne	PBE				PBE-D3			
	Down		Up		Down		Up	
	E_{ads}	E_b	E_{ads}	E_b	E_{ads}	E_b	E_{ads}	E_b
[1],[1,2]{0,1}	-0.00	—	-0.00	—	-0.03	—	-0.04	—
[2],[1,2]{0,1}	-0.00	—	-0.00	—	-0.03	—	-0.05	—
[3],[1,2]{0,1}	-0.00	—	-0.00	—	-0.04	—	-0.05	—

Table 5: Adsorption, E_{ads}, and penetration energy barriers, E_b, of CH_4, for different grazyne membrane *c(2×2)* models. All values are given in eV.

This is the reason why E_b values are not shown in Table 5, since the values obtained for the TSs do not allow one calculating the penetration energy barriers. Furthermore, apart from moving the CH_4 away from the membrane, the latter also bulges a bit as happened with parallel CO_2 calculations. These facts indicate that the CH_4 molecule is too large to pass through the acetylenic pores of [3],[1,2]{0,1}-, 3],[1,2]{0,1}- and [3],[1,2]{0,1}-grazynes, so the methane diffusion process is not expected to take place.

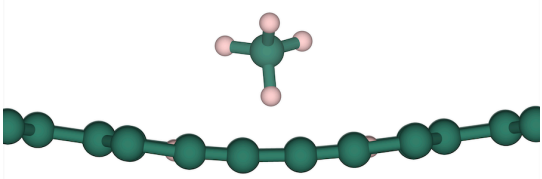

Figure 19: Example of a CH_4 TS calculation for the [3],[2]{1}-grazyne. Carbons and Hydrogen atoms are shown as green and white spheres, respectively.

7.2.1.1. Penetration Barrier Study

Although it seems that de diffusion process will not occur for the CH_4 systems, the study of the penetration barrier profiles has been carried out. As for CO_2, calculations started with a CH_4 placed 5 Å away from the grazyne and then the distance was progressively decreased until 0.1 Å. In Table 6 all the adsorption energies with their respective heights are listed. One realizes that energy increases when the height decreases, however, these values cannot be read in this way. As above explained, the larger molecule size of methane makes the diffusion process more difficult to occur and, as happened with parallel CO_2 systems, when the adsorbate CH_4 is close to the surface, the latter suffers a bulging process, as shown exemplarily in Figure 19.

	PBE			**PBE-D3**		
h	**Down**					
	[1],[1,2] {0,1}	**[2],[1,2] {0,1}**	**[3],[1,2] {0,1}**	**[1],[1,2] {0,1}**	**[2],[1,2] {0,1}**	**[3],[1,2] {0,1}**
5	-0.00	-0.00	-0.00	-0.03	-0.03	-0.04
4	-0.01	-0.01	-0.01	-0.07	-0.08	-0.09
3	-0.01	-0.00	-0.00	-0.14	-0.14	-0.13
2	0.04	0.06	0.07	-0.15	-0.12	-0.12
1.5	0.12	0.14	0.16	-0.08	-0.05	-0.06
1	0.25	0.31	0.26	0.05	0.01	0.10
0.7	0.38	0.38	0.41	0.17	0.16	0.18
0.4	0.51	0.46	0.57	0.35	0.26	0.28
0.1	0.56	—	—	0.53	—	—

Table 6: Adsorption energies, E_{ads}, of down CH_4 at different heights of grazyne. Heights are given in Å while energies in eV.

Hence, the obtained energy values do not correspond to the real distances because grazyne moves away from methane. Notice that in Table 7 not all heights, *h*, feature an E_{ads} value, because during the process of optimization the system evolved to other structures given the high energy of the alleged TS state, see the case of [3],[1,2]{0,1}-grazyne in PBE-D3 calculations in Figure 20. There, the CH_4 placed perturbs the grazyne structure affecting other acetylenic holes that forms stripes of seven and five rings. On the other hand, and as happened in almost all other calculations, PBE-D3 obtained lower energy values than PBE, being here lower by 0.30 eV at most. Both bulging process and structure deformation most probably indicate that the pore size is too small for methane to pass across it.

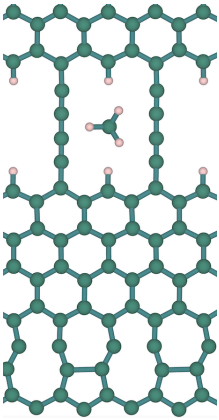

Figure 20: Top view of [3],[1,2]{0,1}-grazyne with an initial distance between adsorbate and substrate of 0.1 Å. Colour code as in Figure 19.

Following the same process as above, the values listed in Table 7 were obtained for CH_4 with the H atom pointing up. When one studies the values listed in Table 7, they reaffirm what has already been above mentioned. The energetic values are low but, as for down methane, grazyne structures bulge, because the high repulsion, when the adsorbate is close, so the values do not accurately represent the positions where the methane was placed. In addition, as the reader can observe, there are also systems without energy values since the structures have been deformed during the optimization process, see Figure 21. In them two important thinks can be noticed; firstly, the transformation of acetylenic linkages in rings of seven and five carbons and, secondly, CH_4 was initially placed with the hydrogen up, while, during the optimization, it undergoes a rotation placing such hydrogen direction to the grazyne. Besides, these grazyne structures also suffer bulging caused by the high repulsion between adsorbate and substrate.

	PBE			PBE-D3		
h				**Up**		
	[1],[1,2] {0,1}	**[2],[1,2] {0,1}**	**[3],[1,2] {0,1}**	**[1],[1,2] {0,1}**	**[2],[1,2] {0,1}**	**[3],[1,2] {0,1}**
5	-0.00	-0.00	-0.00	-0.04	-0.05	-0.05
4	-0.01	-0.01	-0.01	-0.8	-0.08	-0.08
3	-0.01	-0.01	-0.01	-0.14	-0.15	-0.15
2	0.06	0.07	0.08	-0.12	-0.12	-0.11
1.5	0.18	0.18	0.19	-0.02	-0.02	-0.02
1	0.37	0.32	0.36	0.20	0.12	—
0.7	0.52	0.47	—	0.29	0.24	—
0.4	0.65	—	—	—	—	—
0.1	1.32	—	—	—	—	—

Table 7: Adsorption energies, Eads, of up CH4 at different heights from grazyne. Distances are given in Å while energies in eV.

Thus, in general, there is not a very high difference between the values obtained for down and up CH_4, despite it is observed that structures with a methane H up give rise to unwanted systems at a greater distance than with a methane H atom pointing down.

Once the study of these methane systems has been performed, it seems as none of the grazyne structures are capable of permeating CH_4. The main reason for this is that the pore size studied is too small for the CH_4 molecule to pass through, displaying either too high E_b barriers, or large deformation of the substrate structure. This is a valid point as such defective structures allow diffusing CO_2 with moderate E_b values, while none of them displays a great affinity towards neither CO_2 nor CH_4. Thus, such membranes could well be capable of filtering CO_2 and not CH_4, enriching the CH_4 content of the input flux gas stream, and effectively upgrading the biogas.

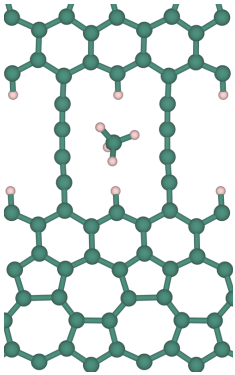

Figure 21: Top view of [1],[2]{1}-grazyne with an initial distance between adsorbate and substrate of 0.4 Å. Colour code as in Figure 19.

7.3. RATE CONSTANTS

Once it has been determined that [1],[1,2]{0,1}, [2],[1,2]{0,1}, and [3],[1,2]{0,1}-grazynes are capable of filtering perpendicular CO_2, a study of the rate constants at different temperatures has been carried out using the vibrational frequencies computationally calculated and applying Eq. (11). The obtained values, for systems with CO_2 placed perpendicular to the grazyne on each compound are represented in Figure 22. In it, it is possible to realize that PBE-D3 calculations have major rate constants comparing with PBE. At low temperatures values show that rate constants are relatively low but when the temperature increases, rate constants increase in a high proportion.

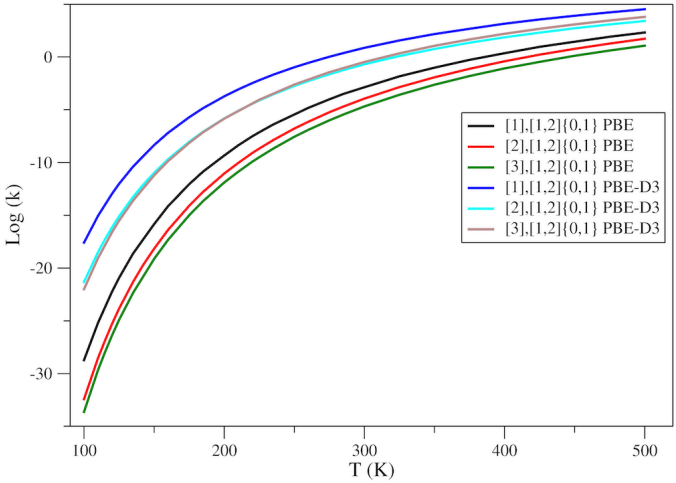

Figure 22: Representation of the variation with temperature of the rate constant logarithm as found in the studied structures.

As above stated, the PBE-D3 energy barriers for CO_2 diffusion were smaller than PBE ones by *ca.* 0.25 eV. This is translated in Figure 22 with *k* values that are sensibly larger for PBE-D3 calculations than for PBE ones, by easily a couple of orders of magnitude at moderate temperatures of 400 K. This highlights the high effect that the accuracy on the E_b values has on the rate constants, and here specifically, on how dispersive forces affect the transition state stabilization. Finally, the [1],[1,2]{0,1}-grazyne appears to be the most suited explored case for CO_2 to trespass, and so, for an effective biogas upgrading.

7.3.1. Selectivity

It was explained in Eq. (14) that the selectivity of CO_2 diffusion through the grazyne membrane compared to CH_4 could be calculated. After studying all the values obtained for both molecules, it is clear that perpendicular CO_2 will pass through the grazyne membrane while any of the studied grazyne structures is impermeable to CH_4, as forcing it to get close the grazyne results in high-energy systems, that evolved in great distortions of the substrate, or even the decomposition of the molecule. Furthermore, CH_4 calculations reveal that the high energy between methane and membrane makes the latter bulge, just as a relaxation mechanism avoiding the contact with CH_4. One could visualize this dynamically as a CH_4 molecule approaching the grazyne net, that, upon contact, elastically deforms, absorbing the kinetic energy, just to recover back its shape, expelling back the CH_4 molecule into the vacuum; very much a nanoscopic view of a tennis ball bouncing out a tennis racket. This means that CH_4 will never trespass the membrane and, hence, the diffusion through process will not occur. Given this, one can conclude that the selectivity of CO_2 will be of 100% over CH_4 for these studied grazynes.

On the other hand, parallel CO_2 is not going to be filtered for two main reasons. First of all, at the time of calculating the TS, the lineal structure of CO_2 distorts evolving it to a structure with a 102º angle between oxygens and carbon and, apparently, forming a bond with the grazyne surface. Secondly, as occurred with CH_4 optimizations, the high repulsion between adsorbate and substrate makes the latter bulged and parallel CO_2 repelled. All of this allows one to think that the selectivity of perpendicular CO_2 over parallel CO_2 will be of 100%, being the perpendicular diffusion mechanism the only viable procedure of permeating the grazyne membrane.

8. CONCLUSIONS

Once all the results have been obtained and discussed, the following particular conclusions can be listed:

- As one increases the acetylenic pore size, both the adsorption and penetration barrier energies for both CO_2 and CH_4 molecules decrease.
- Both CO_2 and CH_4 physisorb on the studied grazynes, displaying small adsorption energy values.
- Perpendicular CO_2 is found to be filtered in [1],[1,2]{0,1}, [2],[1,2]{0,1} and [3],[1,2]{0,1}-grazynes, the compounds with the largest acetylenic pore studied in this project. Filtration is found to be not possible when having smaller pores.
- Neither parallel CO_2 nor CH_4 is filtered in the above studied cases, as high repulsions between substrate and adsorbate are found, capable of modifying or even breaking systems by transforming it into unwanted structures.
- Graphene width does not have a significant effect on the studied diffusion process since the energy values obtained are similar for three systems, although a slight increase in energy has been observed as the width increases.
- PBE-D3 results display more negative E_{ads} values, and lower energy barriers than PBE, with a strong impact in the diffusion rate constants.
- The selectivity of perpendicular CO_2 over CH_4 in [1],[1,2]{0,1}, [2],[1,2]{0,1} and [3],[1,2]{0,1}-grazynes is theoretically of 100%, as a result that no structure is capable to filter methane.

9. REFERENCES

1. Feichter, J.; Schurath, U.; Zellner, R. A. Luftchemie und Klima. *Chemie Unserer Zeit* **2007**, *41*, 138-150.
2. Kunkel, C.; Viñes, F.; Illas, F. Biogas Upgrading by Transition Metal Carbides. *ACS Appl. Energy Mater.* **2018**, *1*, 43-47.
3. Prats, H.; Mcaloone, H.; Viñes, F.; Illas, F.: Ultra-High Selectivity Biogas Upgrading through Porous MXenes. *J. Mater. Chem. A* **2020**, *8*, 12296-12300.
4. Chen, J. J.; Li, W. W.; Li, X. L.; Yu, H. Q.: Improving Biogas Separation and Methane Storage with Multilayer Graphene Nanostructure *via* Layer Spacing Optimization and Lithium Doping: A Molecular Simulation Investigation. *Environ. Sci. Technol.* **2012**, *46*, 10341-10348.
5. Covarrubias-García, I.; Quijano, G.; Aizpuru, A.; Sánchez-García, J. L.; Rodríguez-López, J. L.; Arriaga, S. Reduced Graphene Oxide Decorated with Magnetite Nanoparticles Enhance Biomethane Enrichment. *J. Hazard. Mater.* **2020**, *397*, 122760.
6. Kang, J.; Wei, Z.; Li, J. Graphyne and Its Family: Recent Theoretical Advances. *ACS Appl. Mater. Interfaces* **2019**, *11*, 2692–2706.
7. Kamalinahad, S.; Viñes, F.; Gamallo, P. Grazynes: Carbon-Based Two-Dimensional Composites with Anisotropic Properties. *J. Phys. Chem. C* **2019**, *123*, 27140-27149.
8. Kohn, W.; Sham, L. J. Self-Consistent Equations Including Exchange and Correlation Effects. *Phys. Rev. A* **1965**, *120*, 23698-23706.
9. Hohenberg, P.; Kohn, W. Inhomogeneous Electron Gas. *Phys. Rev.* **1964**, *136*, 864.
10. Perdew, J. P. Jacob's Ladder of Density Functional Approximations for the Exchange-Correlation Energy. *AIP Publishing* **2003**, 1-20.
11. Perdew, J. P.; Burke, K.; Ernzerhof, M. Generalized Gradient Approximation Made Simple. *Phys. Rev. Lett.* **1996**, *78*, 1396.
12. Novoselov, K. S.; Geim, A.; Morozov, S. V.; Jiang, D.; Zhang, Y.; Dubonos, S. V.; Grigorieva, I. V.; Firsov, A. A. Electric Field in Atomically Thin Carbon Films. *Science* **2004**, *80*, 666-669.
13. Tiwari, S. K.; Sahoo, S.; Wang, N.; Huczko, A. Graphene Research and their Outputs: Status and Prospect. *J. Sci. Adv. Mater. Devices,* **2020**, *5*, 10–29.
14. Moreno, C.; Vilas-Varela, M.; Kretz, B.; Garcia-Lekue, A.; Costache, M. V.; Pardinas, M.; Panighel, M.; Ceballos, G.; Valenzuela, S. O.; Peña, D.; Mugarza, A. Bottom-Up Synthesis of Multifunctional Nanoporous Graphene. *Science* **2018***, 360*, 199-203.
15. Sofo, J. O.; Chaudhari, A. S; Barber, G. D. Graphane: A Two-Dimensional Hydrocarbon. *Phys. Rev. B* **2007**, *75*, 153401.
16. Peng, Q.; Dearden, A. K.; Crean, J.; Han, L.; Liu, S.; Wen, X.; De, S. New Materials Graphyne, Graphdiyne, Graphone, and Graphane: Review of Properties, Synthesis, and Application in Nanotechnology. *Nanotechnol. Sci. Appl.* **2014**, 7, 1-29.
17. Baughman, R. H.; Eckhardt, H.; Kertesz, M. Structure-Property Predictions for New Planar Forms of Carbon: Layered Phases Containing sp^2 and *sp* Atoms. *J. Chem. Phys.* **1987**, *87*, 6687.
18. Malko, D.; Neiss, C.; Viñes, F.; Görling, A. Competition for Graphene: Graphynes with Direction-

Dependent Dirac Cones. *Phys. Rev. Lett.* **2012**, *108*, 8-24.

19. Puigdollers, A. R.; Alonso, G.; Gamallo, P. First-Principles Study of Structural, Elastic and Electronic Properties of α-, β-, and γ-Graphyne. *Carbon* **2016**, *96*, 879-887.
20. Kresse, G.; Furthmüller, J. Efficient Iterative Schemes for *Ab Initio* Total-Energy Calculations Using a Plane-Wave Basis Set. *Phys. Rev. B* **1996**, *54*, 11169-11186.
21. Blöchl, P. E. Projector Augmented-Wave Method. *Phys. Rev. B* **1994**, *50*, 17953-17979.
22. Grimme, S.; Antony, J.; Ehrlich, S.; Krieg, H. A Consistent and Accurate Ab Initio Parametrization of Density Functional Dispersion Correction (DFT-D) for the 94 Elements H-Pu. *J. Chem. Phys.* **2010**, *132*, 154104.
23. Fu, Y.; Ragab, T.; Basaran, C. The Effect of Stone-Wales Defects on the Mechanical Behavior of Graphene Nanoribbons. *Comput. Mater. Sci.* **2016**, *124*, 142-150.

10. ACRONYMS

CI: Configuration Interactions

DFT: Density Functional Theory

fcc: face-centered cubic

GGA: Generalized Gradient Approximation

HF: Hartree-Fock

LDA: Local Density Approximation

MP: Møller-Plesset

PAW: Projector Augmented Wave

PBC: Periodic Boundary Conditions

PBE: Perdew-Burke-Ernzerhof

TS: transition state

VASP: Vienna Ab initio Simulation Package

vdW: van der Waals

xc: exchange-correlation